Wave Optics Based LEO-LEO Radio Occultation Retrieval

von Benzon, Hans-Henrik; Høeg, Per

Published in:
Radio Science

Link to article, DOI:
10.1002/2015RS005852

Publication date:
2016

Document Version
Peer reviewed version

Wave Optics Based LEO-LEO Radio Occultation Retrieval

Hans-Henrik Benzon (hhvb@space.dtu.dk), Per Høeg (hoeg@space.dtu.dk)

The Technical University of Denmark, Space Division, Elektrovej Building 328, 2800 Kgs. Lyngby Denmark

1. Abstract

This paper describes the theory for performing retrieval of radio occultations that use probing frequencies in the XK and KM band. Normally radio occultations use frequencies in the L band and GPS satellites are used as the transmitting source and the occultation signals are received by a GPS receiver on board a Low Earth Orbit (LEO) satellite. The technique is based on the Doppler shift imposed, by the atmosphere, on the signal emitted from the GPS satellite. Two LEO satellites are assumed in the occultations discussed in this paper and the retrieval is also dependent on the decrease in the signal amplitude caused by atmospheric absorption. The radio wave transmitter is placed on one of these satellites while the receiver is placed on the other LEO satellite. One of the drawbacks of normal GPS based radio occultations is that external information is needed to calculate some of the atmospheric products such as the correct water vapor content in the atmosphere. These limitations can be overcome when a proper selected range of high frequency waves are used to probe the atmosphere. Probing frequencies close to the absorption line of water vapor have been included, thus allowing the retrieval of the water vapor content. Selecting the correct probing frequencies would make it possible to retrieve other information such as the content of ozone. The retrieval is performed through a number of processing steps which are based on the Full Spectrum Inversion (FSI) technique. The retrieval chain is therefore a wave optics based retrieval chain and it is therefore possible to process measurements that include multipath. In this paper simulated LEO to LEO radio occultations based on 5 different frequencies are used. The 5 frequencies are placed in the XK or KM frequency band. This new wave optics based

retrieval chain is used on a number of examples and the retrieved atmospheric parameters are compared to the parameters from a global ECMWF analysis model. This model is used in a forward propagator that simulates the electromagnetic field amplitudes and phases at the receiver on board the LEO satellite.

LEO-LEO cross-links radio ooccultations using high frequencies are a relative new technique and the possibilities and advantages of the technique still needs to be investigated. The retrieval of this type of radio occultations is considerable more complicated than standard GPS to LEO radio occultations, because the attenuation of the probing radio waves is used in the retrieval and the atmospheric parameters are found using a least square solver. The best algorithms and the number of probing frequencies that is economical viable must also be determined. This paper intends to answer some of these questions using end to end simulations.

2. Introduction

It is well known from the literature that GPS-LEO radio occultation sounding can lead to derivation of atmospheric parameters like temperature, pressure and humidity, based on the bending of the emitted signal due to variations in the refractive index, see [*Benzon et al.,* 2015]. These data are increasingly considered for numerical weather prediction and climate models. Space missions such as GPS/MET, CHAMP and METOP clearly indicate that temperature in large part of the atmosphere can be estimated with an accuracy of 1 K. However, when it comes to determination of humidity in the atmosphere based on GPS-LEO measurements, there is a need for a priori estimates of the temperature. Water vapor is a major greenhouse gas and due to its large abundance, it significant influences the climate. Also, due to the large energy transfers associated with the phase transitions of water it impacts the short term dynamics of the atmosphere considerably e.g. by stimulating the development of tropical hurricanes. Therefore, an accurate knowledge of the temporal and spatial water vapor distribution is desirable. In order to avoid use of external data more sophisticated satellite systems have been proposed where the atmosphere is sounded through LEO-LEO cross-links [*Høeg and Kirchengast,* 2002, *Kursinski et al.*, 2002; *Eriksson et al.*, 2003]. The carrier frequencies used in these LEO-LEO links must be located around a water vapor absorption line to enable detection of both phase and amplitude modulations caused by the atmosphere.

It is essential, for each probing frequency, to correctly retrieve the complex refraction index [*Schweitzer et al*. 2011]. This paper also contains end to end simulations for LEO-

LEO links using 3 or 5 probing radio waves with frequencies near absorption lines. The retrievals are based on bending angle and transmission profiles calculated from geometric optics while the atmospheric state variables are calculated using the iterative Best Linear Unbiased Estimation (BLUE) algorithm. A discussion of important GPS radio occultation and LEO-LEO cross link missions and proposals can also be found in the paper. Under the assumption of spherical symmetry, a complex refractivity profile is readily computed, through Abel transforms, from a profile of bending angle and a profile of transmission (optical depth) measured as functions of ray impact parameter [*Kursinski et al*. 2002]. Wave optics based retrieval techniques such as Full Spectrum Inversion (FSI), Canonical Transform CT or geometric optics can be used to calculate the bending angle and transmission height profiles. [*Kursinski*, 2002] describes how transmission profiles can be computed using geometrical optics whereas [*Gorbunov*, 2002] suggests the use of the canonical amplitude in order to establish the transmission profile. The major advantage of wave optics based methods as compared to geometrical optics is that the former methods can disentangle multipath [*Gorbunov*, 2002, *Jensen et al.* 2003 and *Jensen et al.* 2004]. This disentanglement of multipath gives a lower noise level in the retrieved parameters in case of multipath. A wave optics based retrieval chain based on FSI will be used in this study.

Alternatively, atmospheric parameters can also be derived from observations of the variations in the absorption coefficient with frequency by using pairs of frequencies (calibrations frequencies/tones) [*Kursinski et al.* 2002, *Nielsen et al*. 2003, *Gorbunov et. al.* 2007]. In this approach atmospheric parameters are derived from a profile of real

refractivity plus measured variations in imaginary refractivity as function of frequency. These variations are computed by an Abel transform, assuming spherical symmetry, of a profile representing the differences between two absorption profiles computed at two different frequencies.

Improved RO satellite missions with potential of determination of both temperature and humidity without a priori information has been proposed, see [*Høeg and Kirchengast*, 2002] and the needed retrieval techniques have been presented [*Kursinski et al.*, 2002 and *Gorbunov et. al.,* 2005]. In the simulation study presented here, we simulate the concept of using 5 different frequencies in the XK and KM frequency band respectively. The radio occultation's are performed by two LEO satellites one of them transmitting radio signals at 5 different frequencies. By measuring not only the phase but also the amplitude variations of the signals unambiguous retrieval of temperature, pressure and humidity profiles is made possible. Key components of this new LEO-LEO retrieval chain is the FSI and the trust-region solver that calculates the atmospheric parameters from the complex refractivity's. A statistical analysis performed on the simulations reveals the level of accuracy and precision that can be expected from the technique.

3. Retrieval of LEO-LEO radio occultations

This section presents a discussion of the wave optics based LEO-LEO retrieval chain. The atmospheric propagation of the LEO-LEO signals and the data analysis is studied using a sequence of simulation elements. Each element processes the output of the previous element and generates the input of the following element. In all simulations the refractivity field is assumed to be spherically symmetric, i.e., $N(\vec{r})=N(r)$. The total end to end simulation chain is depicted in Figure 1.

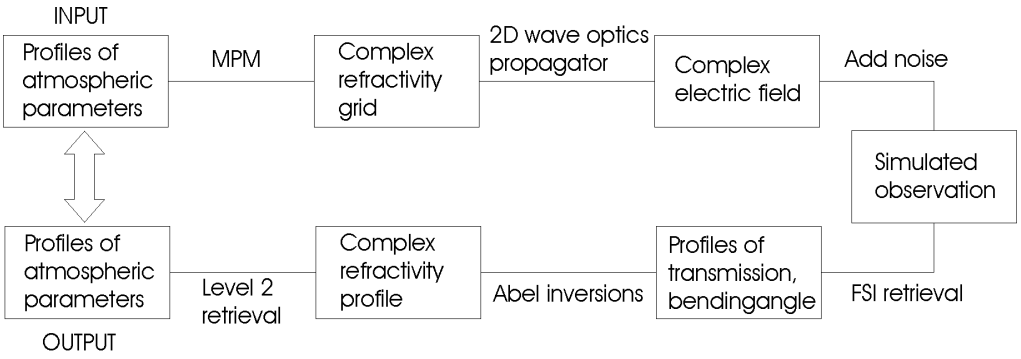

Figure 1. Overview of the simulation processing chain.

First, atmospheric parameter inputs (temperature, pressure and humidity) are transformed to a complex refractivity field using a Millimetre-wave Propagation Model (MPM). Subsequently, this field is applied in the wave optics propagation simulations that yield the electromagnetic field along the receiver orbit. These fields are used as the starting point for the retrieval. The retrieval starts by calculating the bending angle and transmission profiles for each of the probing frequencies using the Full Spectrum

Inversion (FSI) technique. These profiles are then inverted into complex refractivity profiles through Abel inversions. Finally, the profiles of atmospheric parameters are retrieved through a non-linear least square fit. In the following, these different processing steps are described.

Retrieval of bending angle and transmission based on FSI

Our retrieval scheme is based on the Full Spectrum Inversion (FSI) method [*Jensen et al.* 2003]. The FSI technique applies a Fourier transform and uses the derivative of the phase after this transformation. Time and instantaneous frequency are the output from FSI – also in case of multipath, where there will be more Doppler frequencies at a given time. The Fourier amplitudes describe the distribution of energy with respect to impact parameter only modulated by signal spreading and absorption, i.e., defocusing is automatically accounted for.

When using Full Spectrum Inversion to invert radio occultation data, a distinction between ideal occultations and realistic occultations must be made. Ideal occultations are defined as occultations with a spherical Earth and perfect circular orbits lying in the same plane. On the other hand, realistic occultations are defined as occultations with an oblate Earth and approximately circular orbits lying in two different planes. In the former case, a global Fourier transform can be applied directly to the measured signal; and pairs of ray arrival time, t_0, and ray Doppler angular frequency, ω_0, is related through:

$$(\omega(t_0), t_0) = \left(\omega_0, -\left| \frac{d \arg(F)}{d\omega} \right|_{\omega=\omega_0} \right) \quad (1)$$

where F represents the Fourier transform of the measured signal. Realistic occultations require that the occultation signal and ephemeris data are re-sampled with respect to the opening angle, θ, between the radius vectors of the satellites and that frequency variations caused by radial variations in the radius vectors are removed before the equation above is applied, see [*Jensen et al.* 2003]. When the variations in the Doppler frequency have been determined through equation (1), then the bending angle profile can be found from the standard equations, see e.g. [*Kursinski et al.* 2000].

The corresponding transmission profile is determined by expressing the Fourier amplitudes with respect to impact parameter and by correcting the amplitudes for spreading modulations. The transmission, i.e. the normalized intensity, is related to the ray amplitude data through

$$\xi(a) = \frac{I(a)}{I_m(a)} = \frac{A^2(a)}{A_m^2(a)} \quad (2)$$

where I is the intensity of the signal in the absence of spreading and defocusing, I_m is the intensity the signal would have had without absorption, spreading and defocusing, and A and A_m are the corresponding amplitudes. The Fourier amplitude is related to the occultation geometry through

$$|F(a)|^2 = \xi(a)\frac{P}{2\pi}\cdot\frac{a}{r_G r_L \sin(\theta)\sqrt{r_G^2 - a^2}\sqrt{r_L^2 - a^2}\left(\frac{d\theta}{da}\right)^2 k} \quad (3)$$

[*Jensen et al.* 2003]. Here P is the transmitter power, r_G and r_L are the distances from the center of curvature to the transmitter and receiver, respectively, and θ is the angle between these. This expression is valid in general for a 3-D geometry with circular orbits. For non-circular orbits, additional terms are introduced in (3) as demonstrated in [*Gorbunov and Lauritsen*, 2004]. Since the simulated electromagnetic field is two-dimensional, spreading corrections are only performed for spreading within the occultation plane. Without transverse effects a factor of $a/(r_G r_L \sin(\theta))$ disappear from (3). In this case the Fourier amplitude becomes

$$|F(a)|^2 = \xi(a)\frac{P}{2\pi}\cdot\frac{1}{\sqrt{r_G^2 - a^2}\sqrt{r_L^2 - a^2}\left(\frac{d\theta}{da}\right)^2 k} \quad (4)$$

where the transmitter power P is assumed constant throughout the occultation. From the discussion, it follows that a profile of transmission multiplied by the transmitted power is readily computed through (2) and (4). The transmitted power in the direction of the receiving satellite may not be known with a high accuracy, however, as long as the transmitted power is constant this will not affect the inversion; this will be shown in the following section.

The FSI method has a number of advantages related to Leo-Leo occultations:

- it disentangles multipath
- defocusing is automatically accounted for
- it is simple, both conceptually and computationally

The major drawback of the FSI technique is that it relies on the assumption of local spherical symmetry. When this assumption is not fulfilled, the method may not be able to disentangle multipath. Like other methods based on Fourier Integral Operators, the FSI amplitude always suffers from minor amplitude oscillations caused by Gibb's phenomenon which may cause unwanted artificial oscillations in the retrieved transmission profiles [*Lohmann et al.* 2006 and *Gorbunov et al.* 2004]. The problem of Gibb's phenomenon can be solved by using appropriate window functions in the evaluation of the Fourier transform as described in [*Lohmann et al.* 2006].

Retrieval of complex refractivity

Given profiles of bending angle and transmission as function of impact parameter the complex refractivity is derived. The real part of the refractivity is derived from the bending angle profile using the standard Abel inversion as described in e.g. [*Fjeldbo*, 1971]. Here focus will be on retrieval of the imaginary part of the refractivity, which is directly related to the absorption. The imaginary refractivity is given by

$$N'' = 10^6 \cdot n'' = 10^6 \cdot (2k)^{-1} \cdot \alpha \tag{5}$$

where k is the free space wave number, n'' is the imaginary part of the refractive index and α is the absorption coefficient per unit distance in the medium [*Born and Wolf,* 1999]. The absorption coefficient is calculated using an inverse Abel integral of the signal transmission [*Kursinski et al.*, 2002],

$$\alpha(a) = \frac{1}{\pi} \frac{da}{dr}\bigg|_{a'=a} \int_a^\infty \frac{d \ln \xi}{da} \frac{da'}{\sqrt{a'^2 - a^2}} \tag{6}$$

where r is the ray path perigee distance to the curvature center, a is the impact parameter and ξ is the transmission defined above. From the equation it follows that the transmission enters the Abel integral as the derivative of the logarithm of the transmission. The transmission may, therefore be scaled with any arbitrary constant without affecting the results of the Abel integral. This explains why it is not a problem for the inversion that the transmission derived from FSI is scaled by the unknown transmitted power. The reason for this is that the signal absorption is related to the relative variations in the signal intensity and not the absolute variations. Consequently, there will be no need for calibration of the measured amplitudes, as the observations will not be affected by long-term drifts in the instrument, which makes the technique very suitable for climate monitoring.

Retrieval of atmospheric parameters

Given the retrieved profiles of both real and imaginary refractivity for the 5 frequencies, and assuming hydrostatic balance, a solution for dry pressure, temperature and water vapor pressure can be found. The 5 real refractivity profiles only constitute one piece of independent information as the atmosphere is virtually non-dispersive for the frequency ranges under consideration. Consequently, the system contains 7 pieces of independent information and three unknowns. A least square (LS) fitting method is employed for this over-determined problem. It is worth to notice that if the signals had also been subject to absorption caused by liquid water, e.g. rain, then the system would have contained an additional unknown parameter, liquid water. However, there will also in this case be a slight redundancy in the number of equations.

In order to exploit the information given by the hydrostatic equation in a simple manner, the inversion is started at the topmost layer corresponding to the largest altitudes where reliable observations can be achieved. Boundary conditions for the *"unknown" parameters p, T* and *e* are specified at this level. In the current simulations the "true" atmospheric parameters are used as the upper boundary conditions. These parameters are then used to calculate an initial guess for the solution at the next level below. The initial guess is adjusted through minimization of a set of appropriate functions by the LS algorithm. The functions to be minimized reflect the information contained in the derived refractivity's and the hydrostatic balance assumption. The function representing the hydrostatic balance constraint is implemented using

$$p_i = p_{i-1} + \Delta p \approx p_{i-1} + g \cdot \tilde{\rho}_i \cdot \Delta h_i = p_{i-1} + \frac{g}{2}\left(\frac{p_i}{RT_i} + \frac{p_{i-1}}{RT_{i-1}}\right)(h_i - h_{i-1}) \quad (7)$$

where ideal gas behavior and linear density, ρ, variations between the levels have been assumed. The level index, i, is counted downwards from the topmost level and g is the gravitational acceleration, R is the gas constant, h is geometric height and p is pressure. Equation (7) expresses the bound on the solution at the i'th level imposed by the solution from the level above. By rearranging this expression and including the information from the retrieved refractivity's an error function $J(p_i,T_i,e_i)$ can be constructed. This function must be minimized at each level with respect to the unknowns p_i, T_i and e_i:

$$\begin{aligned} J(p_i,T_i,e_i) = &\left[\left(p_{i-1} + \frac{gp_{i-1}}{2RT_{i-1}}(h_i - h_{i-1})\right) - \left(p_i - \frac{gp_i}{2RT_i}(h_i - h_{i-1})\right)\right]^2 \\ &+ \left(N_i' - N'(p_i,T_i,e_i)\right)^2 \\ &+ \left(N_{i,1}'' - N''(p_i,T_i,e_i,f_1)\right)^2 \\ &+ \left(N_{i,2}'' - N''(p_i,T_i,e_i,f_2)\right)^2 \\ &+ \left(N_{i,3}'' - N''(p_i,T_i,e_i,f_3)\right)^2 \\ &+ \left(N_{i,4}'' - N''(p_i,T_i,e_i,f_4)\right)^2 \\ &+ \left(N_{i,5}'' - N''(p_i,T_i,e_i,f_5)\right)^2 \end{aligned} \quad (8)$$

The first line in the error function above represents the squared error in the hydrostatic balance equation. The remaining terms represents the squared differences between the retrieved refractivity's and the corresponding refractivity's derived from the Liebe MPM

model for p_i, T_i and e_i. In the Liebe model the magnetic field, droplet density and rain rate contributions are neglected.

The error function given by (8) is non-linear and is minimized using a non linear trust-region solver. The Trust-Region (TR) algorithms are relatively new iterative methods for solving nonlinear optimization problems. They are widely used in power engineering, finance, applied mathematics, mechanical engineering, and other areas. The TR methods have global convergence and local super convergence, which differentiates them from line search methods and Newton methods. The TR methods have better convergence when compared with widely-used Newton-like methods. The main idea behind a TR algorithm is calculating a trial step and checking if the next values of x belong to the *trust region,* see [*Sorensen* 1982]. Calculation of the trial step is strongly associated with the approximation model, which here is the Liebe model. In the solution procedure the retrieved atmospheric parameters at one level is used as the initial guess at the next level.

During the occultations the signals can get so attenuated that the imaginary refractivity's get so small that the corresponding equations in (8) can not be used. Information from the real refractivity is only lost in the extreme situation where neither of the signals can be measured. The portions of the atmosphere where information from the imaginary refractivity's could be lost are related to very wet or dry regions. In the lower troposphere, it is expected that the 23 GHz (and higher) signal may be completely attenuated due to high concentrations of water vapor - this will especially be the situation in the tropics. In the upper troposphere, the concentration of water vapor is expected to be so low that the

absorption of the signal may not contain any useful information. This may also be the case for the other frequencies in the system when the atmosphere is very dry (for instance in the stratosphere), in these cases it will not be possible to retrieve the concentration of water vapor.

4. XK and KM frequency range radio occultations

A large number of simulations both in the XK and in the KM frequency band have been performed in order to validate the retrieval scheme. The frequencies in the XK range contain three frequencies around the 22 GHz water vapor absorption line and two lower frequencies while the frequencies in the KM range contain the same three frequencies around the 22 GHz water vapor line plus two additional frequencies near the 183 GHz absorption line. These frequencies are selected in accordance with international radio frequency regulations, which forbid use of frequencies directly around line center for active sounding.

The forward simulations have been performed using the End-to-End Generic Occultation Performance Simulation and Processing System version 5 (EGOPS5) software [*Kirchengast et al.* 2007, *Fritzer et al.* 2010]. Two transmitting LEO satellites at a height of 800 km and two counter rotating receiver LEO satellites at a height of 600 km was used to simulate the radio occultations. All of the satellites are assumed to follow a sun synchronous orbit. The atmosphere model used in the simulations was extracted from a global ECMWF analysis for a specific northern hemisphere summer day. In order to simulate the effect of atmospheric turbulence noise is added to the forward modeled excess phase and amplitude. This noise is generated following the principles found in [*Gorbunov and Kirchengast,* 2007]. Noise simulating the observation system errors was also superimposed on the simulated radio occultations. The simulated error sources include thermal noise, drift errors and precise orbit errors. Ionospheric scintillations are

not included in the simulations because the corresponding noise level will be very low due to the high probing frequencies. The atmospheric model used in the forward simulations will for simplicity in the following be called the GRAZ atmosphere model. More details on the forward simulations can be found in [*Schweitzer et al*. 2011].

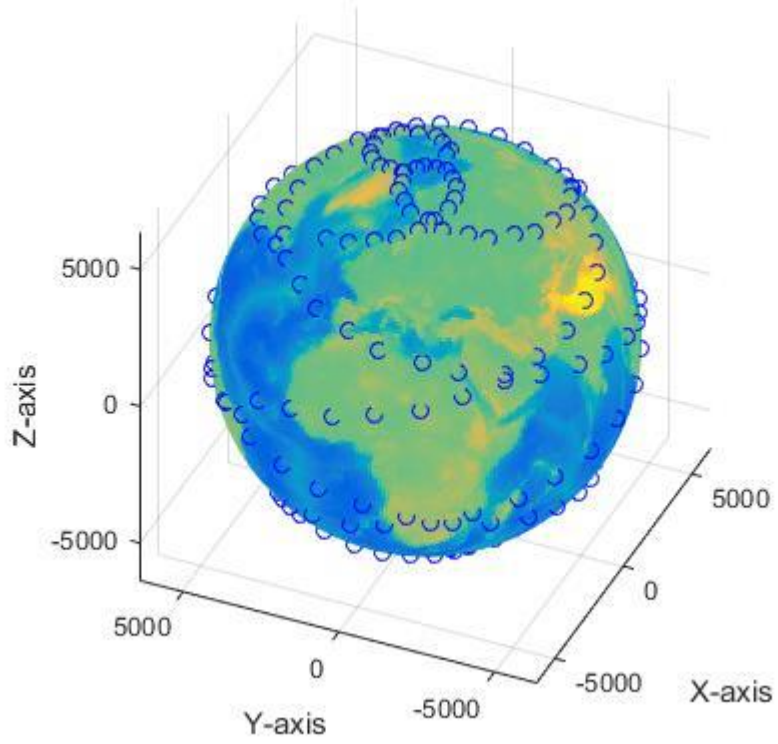

Figure 2**.** Positions of simulated LEO-LEO radio occultations.

The simulations can be classified in the 4 different classes listed below. The positions of the radio occultations can be seen in Figure 2.

1) The forward simulation of the electromagnetic field has been performed in clear air and the electromagnetic field frequencies are in the XK frequency range.

2) The forward simulation of the electromagnetic field has been performed in a cloudy atmosphere that generates atmospheric scintillations. The electromagnetic field frequencies are in the XK frequency range.

3) The forward simulation of the electromagnetic field has been performed in clear air and the electromagnetic field frequencies are in the KM frequency range.

4) The forward simulation of the electromagnetic field has been performed in a cloudy atmosphere that generates atmospheric scintillations. The electromagnetic field frequencies are in the KM frequency range.

101 simulation runs have been performed for each of these classes and a statistical analysis has been performed based on these simulations. The earth is divided into 3 parts corresponding to 3 different latitude intervals. These intervals are tropics 20°S to 20°N, northern hemisphere 30°N to 90°N, and southern hemisphere 90°S to 30°S. The 101 simulation runs for each of the 4 classes is selected in such a way that the 3 latitude intervals are represented equally in the simulations. The table below summarizes the simulations

	Probing radio wave Frequencies	*Meteorological conditions*	*Number of cases*

Simulation Class 1	9 GHZ 13.5 GHz 17.25 GHz 20.2 GHZ 22.6 GHz	Clear air	101
Simulation Class 2	9 GHZ 13.5 GHz 17.25 GHz 20.2 GHZ 22.6 GHz	Turbulent and cloudy air	101
Simulation Class 3	17.25 GHz 20.2 GHz 22.6 GHz 179.0 GHz 181.95 GHz	Clear air	101
Simulation Class 4	17.25 GHz 20.2 GHz 22.6 GHz 179.0 GHz 181.95 GHz	Turbulent and cloudy air	101

Table 1. Simulation classes and the corresponding conditions.

The statistical analysis performed for each of the 4 classes calculates 4 different statistical parameters. These parameters are absolute bias (BIAS), normalized bias (NBIAS), standard error of the difference (SED) and normalized standard error of the difference (NSED). The absolute bias is defined as the mean value of the absolute error and it can be estimated by the follow equation

$$BIAS = \frac{1}{N}\sum_{i=1}^{N}(x_{mi} - x_{vi}) \tag{9}$$

where N is the number samples and x_{vi} and x_{mi} is the i'te sample of the true and measured value respectively.

The normalized bias (NBIAS) is defined as the mean value of the absolute error normalized with respect to the mean true value. This parameter can be estimated with the following equation

$$NBIAS = \frac{\frac{1}{N}\sum_{i=1}^{N}(x_{mi} - x_{vi})}{\frac{1}{N}\sum_{i=1}^{N}x_{vi}} \tag{10}$$

The standard error of the difference (SED) is defined as the standard deviation of the absolute error and is estimated by the following equation

$$SED = \sqrt{\frac{1}{N}\sum_{i=1}^{N}(x_{mi} - x_{vi} - BIAS)^2} \tag{11}$$

The normalized standard error of the difference (NSED) is defined as the standard deviation of the absolute error normalized with respect to the mean value of the true value and is estimated by the following equation

$$NSED = \frac{\sqrt{\frac{1}{N}\sum_{i=1}^{N}(x_{mi} - x_{vi} - BIAS)^2}}{\frac{1}{N}\sum_{i=1}^{N} x_{vi}} \quad (12)$$

The following three subsections contain some of the simulation results performed during the study. The simulation results in the first subsection correspond to simulation class 1 while the simulations in the second subsection correspond to simulations in simulation class 4.

4.1 Comparing XK based retrievals in clear air with corresponding values in the GRAZ model

The forward simulation of the LEO-LEO radio occultation signals has here been performed in clear air. The GRAZ atmosphere model has been used to calculate the complex refractivity field in the forward propagator that simulates the radio occultation measurements. The corresponding pressure, temperature and specific humidity height profiles can also be extracted from the model. These atmospheric height profiles are compared to the retrieved parameters. Results from one of the 101 simulations are presented in Figure 3.

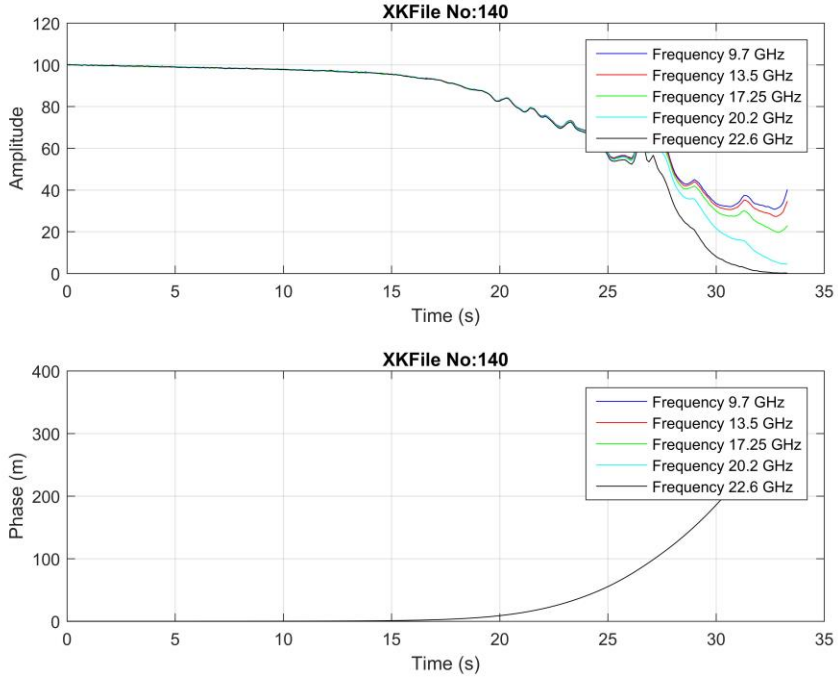

387 (A)

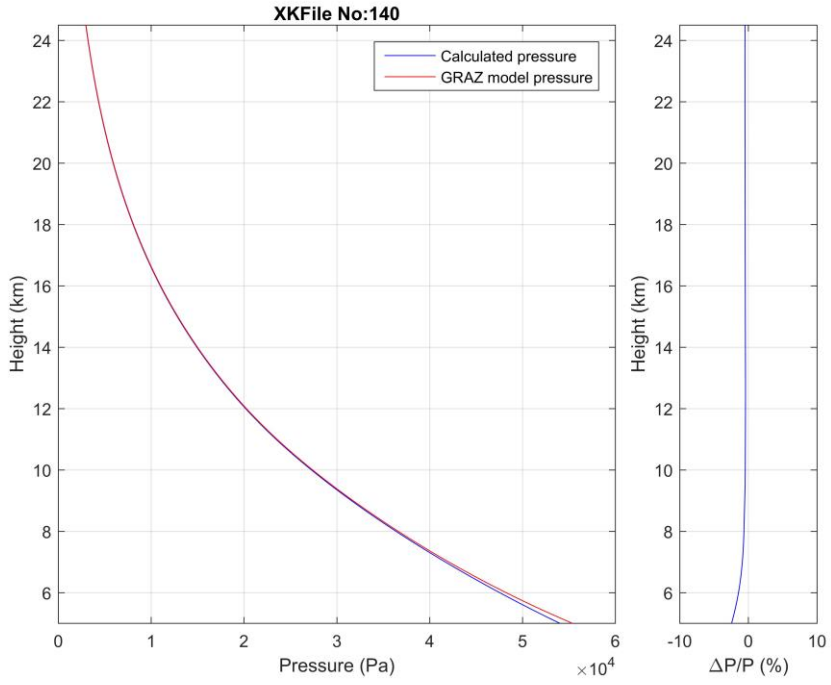

388

389 (B)

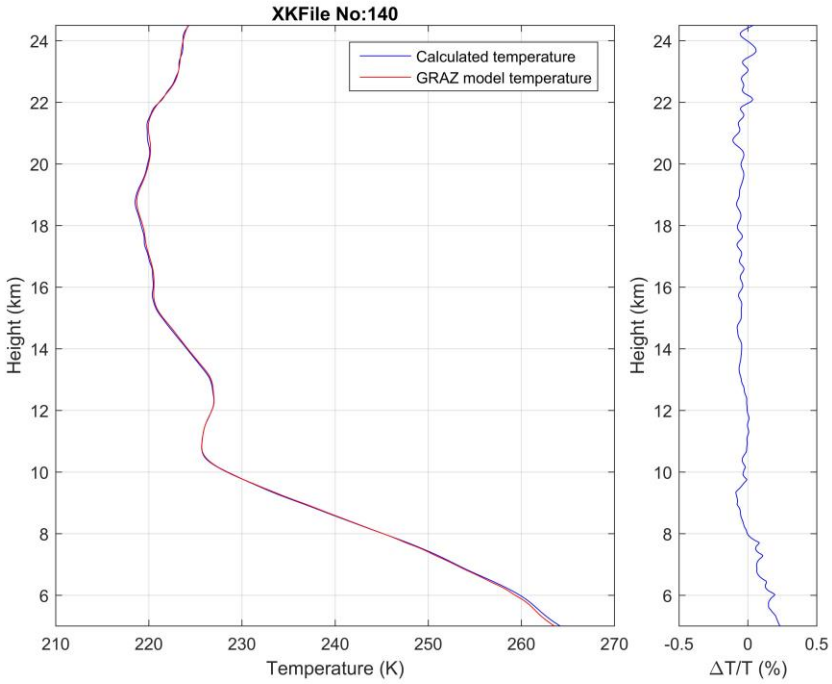

390 (C)

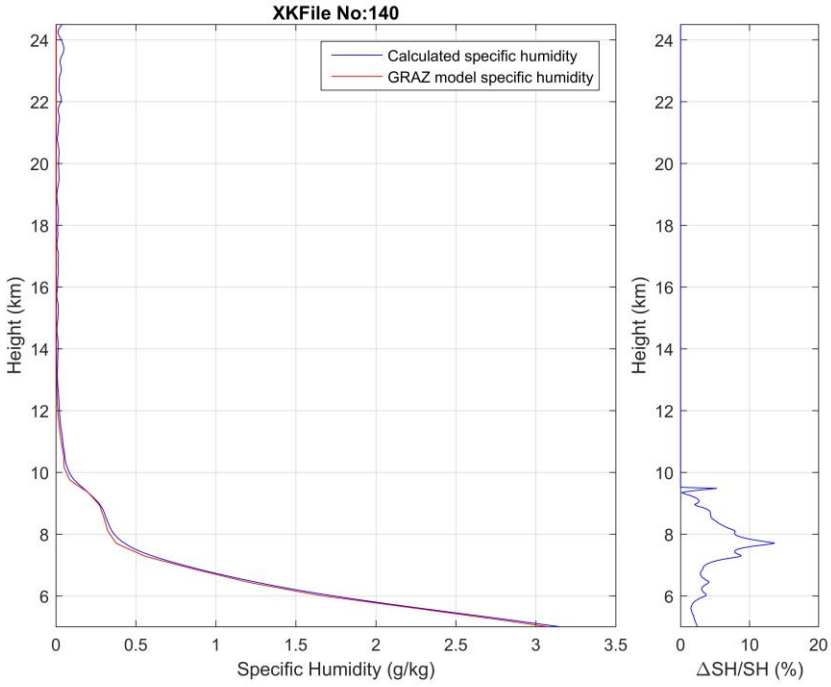

391

392 (D)

Figure 3. (A) The amplitude and phases for the 5 different frequencies. The mean latitude and longitude for the tangent point is 77.86 degrees and 104.02 degrees respectively for this rising occultation. The condition for the simulation is clear air and probing frequencies in the XK range. (B) The pressure versus height. The blue curve is the retrieved pressure while the red curve is the GRAZ model. (C) The temperature versus height. The blue curve is the retrieved temperature while the red curve is the GRAZ model. (D) The specific humidity versus height. The blue curve is the retrieved specific humidity while the red curve is the GRAZ model. Panels (B) to (D) all have a blue curve on the right side which is the relative difference between the retrieved values and the GRAZ model values.

Figure 3 (A) shows the radio occultation amplitudes and phases as a function of time for the 5 probing XK frequencies. These curves are the starting point for the retrieval process. The results of the solver are presented in Figure 2 (B)-(D). These plots show the calculated (blue curve) pressure, temperature and specific humidity profiles together with the corresponding (red curve) model profiles. The relative difference between the retrieved physical parameters and the model values are represented with the blue curves on the right side of the plots. It's seen from the plots that there is a good agreement between retrieved atmospheric parameters and the corresponding model parameters. The specific humidity is in general determined with the lowest precision, but it is still relative precise as long as all of the frequencies are present. The height at which the radio wave is absorbed in the atmosphere decrease with decreasing frequency, so the number of independent equations decrease for heights approaching the earth surface leading to lower

precision in the retrieved parameters. The lowest height in the plots is approximately 5 km, ensuring that all of the probing frequencies are used in the retrieval.

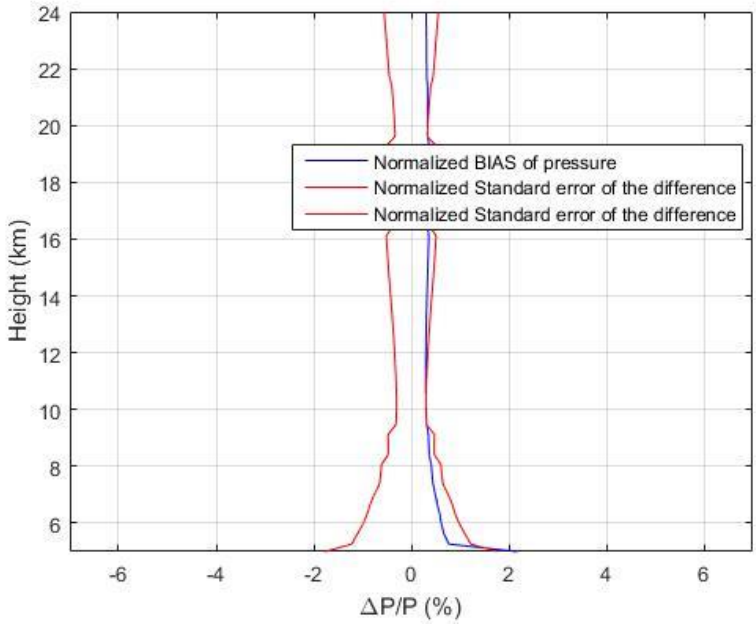

(A)

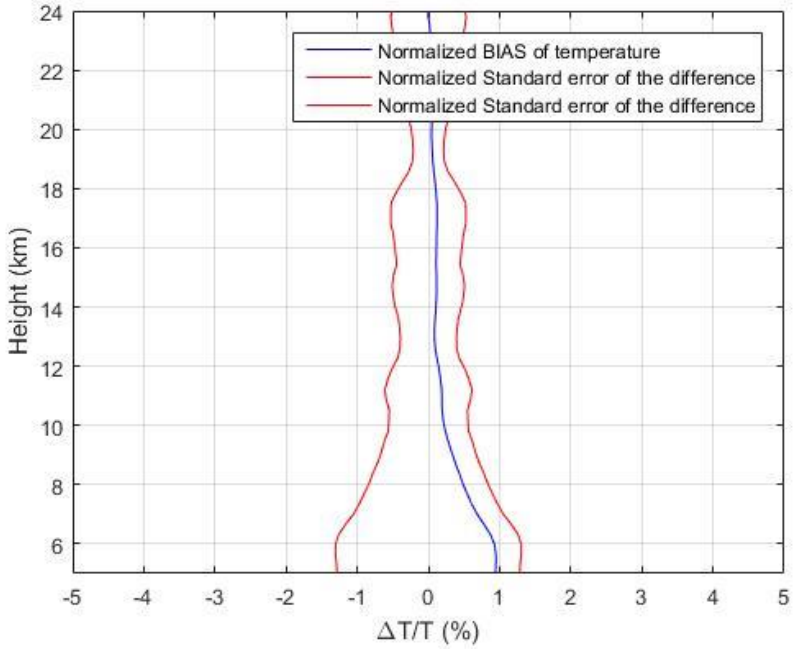

(B)

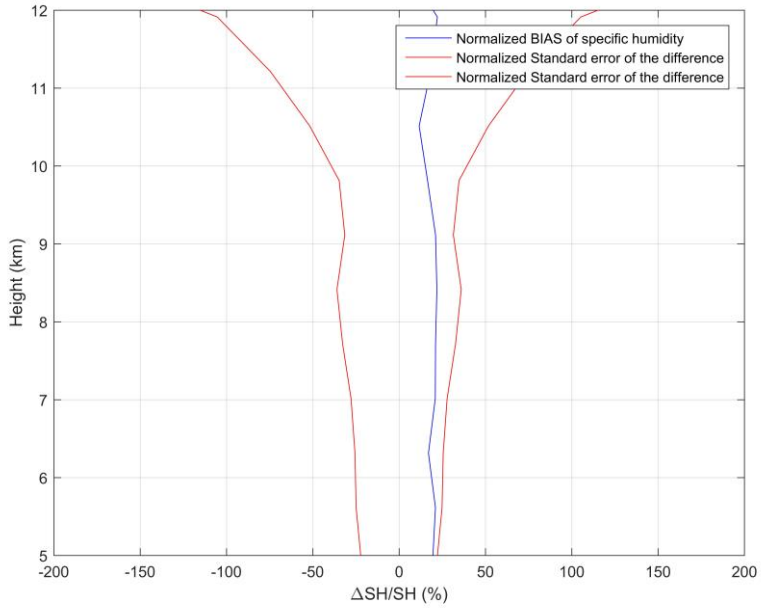

(C)

Figure 4. (A) The normalized pressure bias (blue curve) and normalized standard error of the difference for pressure (red curve) in (%) as a function of height. (B) The normalized temperature bias (blue curve) and normalized standard error of the difference for temperature (red curve) as a function of height. (C) The normalized specific humidity bias (blue curve) and normalized standard error of the difference for specific humidity (red curve) in (%) as a function of height.

Figure 4 shows the result of the statistical analysis. All of the 101 simulations are used in the statistical plots. The statistical analysis is performed for 3 atmospheric parameters, pressure, temperature and specific humidity. The blue curves represent the bias and the red curves represent the standard error of the difference between retrieved and model values. It is seen that the bias and standard error of the difference all fall within an

435 acceptable error level. It is also seen that the bias and standard error of the difference for
436 pressure and temperature are very small at high altitudes but increase for decreasing
437 altitudes. There are not any measurements at low altitudes and the complex refractivity
438 values are therefore found from an extrapolation of the curves. The extrapolated values
439 are found from a polynomial fit to the curves. This will in many cases lead to an error in
440 the retrieved parameters at low altitudes and hence an increase in the bias level.
441
442 Some of the simulations contain multipath. Figure 5 shows such a case. The bending
443 angle profile for one of the XK simulations in clear air is here shown as a function of ray
444 height which is the difference between impact parameter and the local earth curvature. It
445 is seen that all of the probing waves have as expected the same bending angle profile.
446

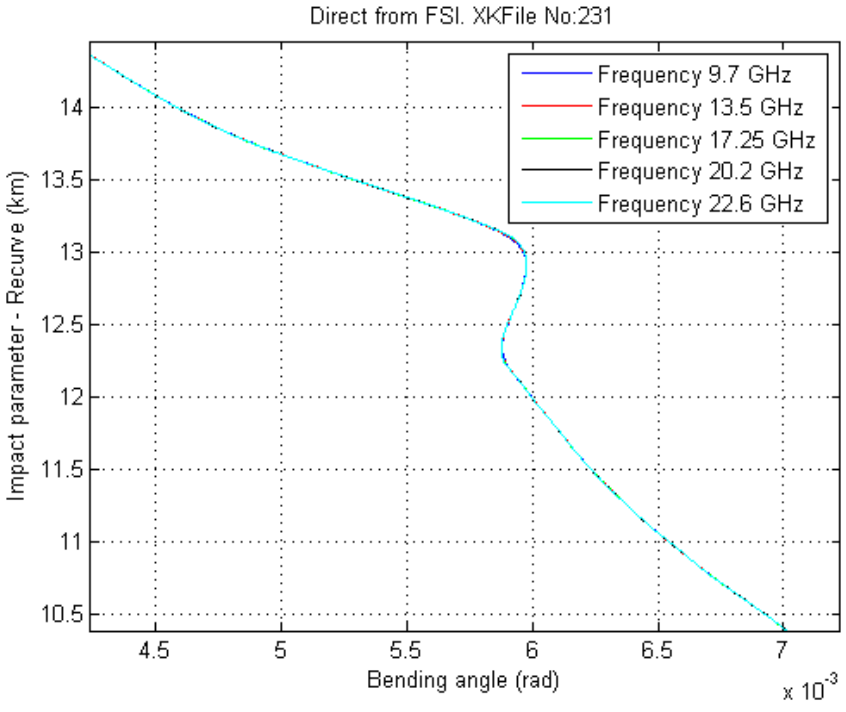

447

448

449 **Figure** 5**.** Closer look at the bending angle versus impact parameter for the 5 frequencies
450 calculated using FSI. The bending angle profiles show the characteristic S-signature
451 which is a sign of multipath.

452

453 The bending angle profiles show the characteristic S-signature which is a sign of
454 multipath. Using a wave optics based retrieval scheme such as FSI insures that the
455 multipath can be correctly resolved.

456

457 **4.2 Comparing KM based retrievals in turbulent and cloudy air with corresponding**
458 **values in the model**

459 The forward simulation of the Leo-Leo radio occultation signals has here been performed
460 in turbulent and cloudy air for probing electromagnetic frequencies in the KM range.
461 Figure 6 (A) shows the amplitudes and phases for the 5 frequencies. It is seen especially
462 on the amplitudes that the signals are noisy due to scintillations caused by the cloudy
463 atmosphere. The result of the solver is presented in Figure 6 (B)-(D). These figures show
464 the calculated (blue curve) pressure, temperature and specific humidity profiles together
465 with the corresponding GRAZ (red curve) model profiles. The relative difference
466 between the retrieved physical parameters and the model values are represented with the
467 blue curves on the right side of the plots. It's seen from the plots that there is a relative
468 good agreement between retrieved atmospheric parameters and the model parameters
469 even for simulations in cloudy air.

470

471

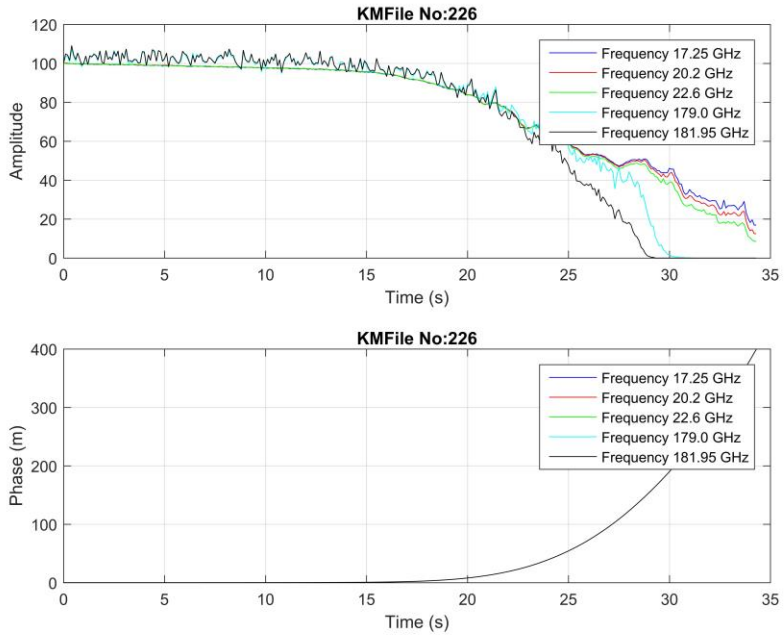

472 (A)

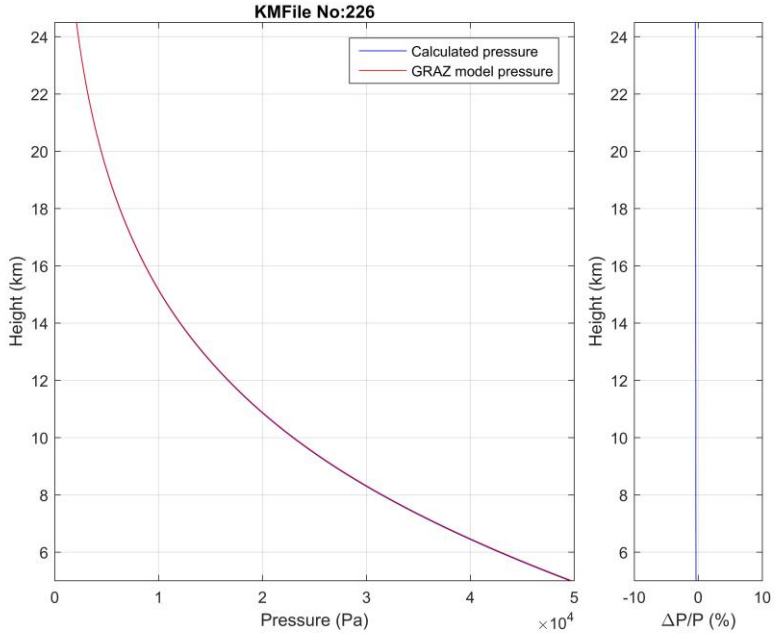

473

474 (B)

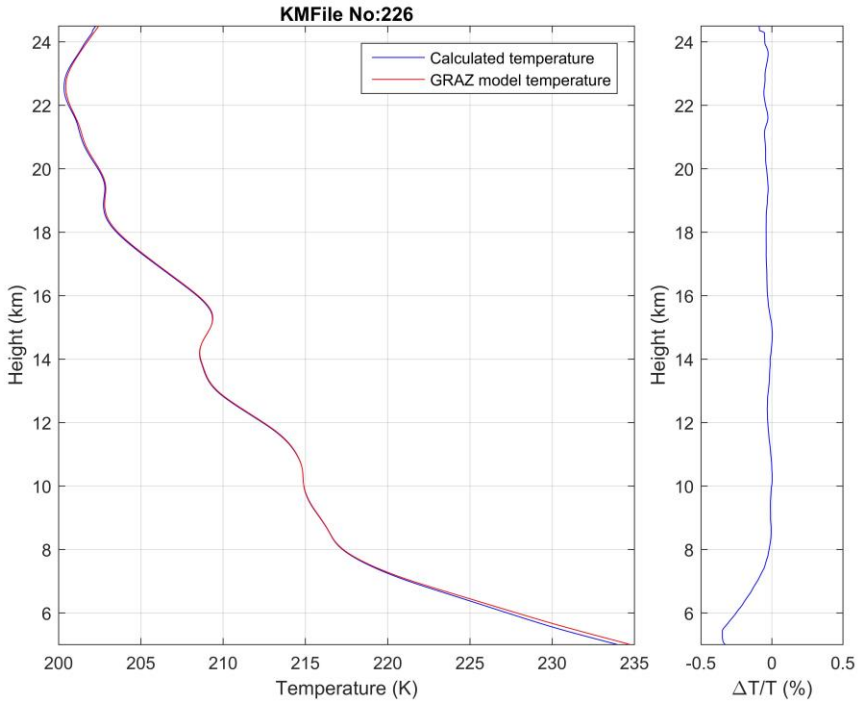

475 (C)

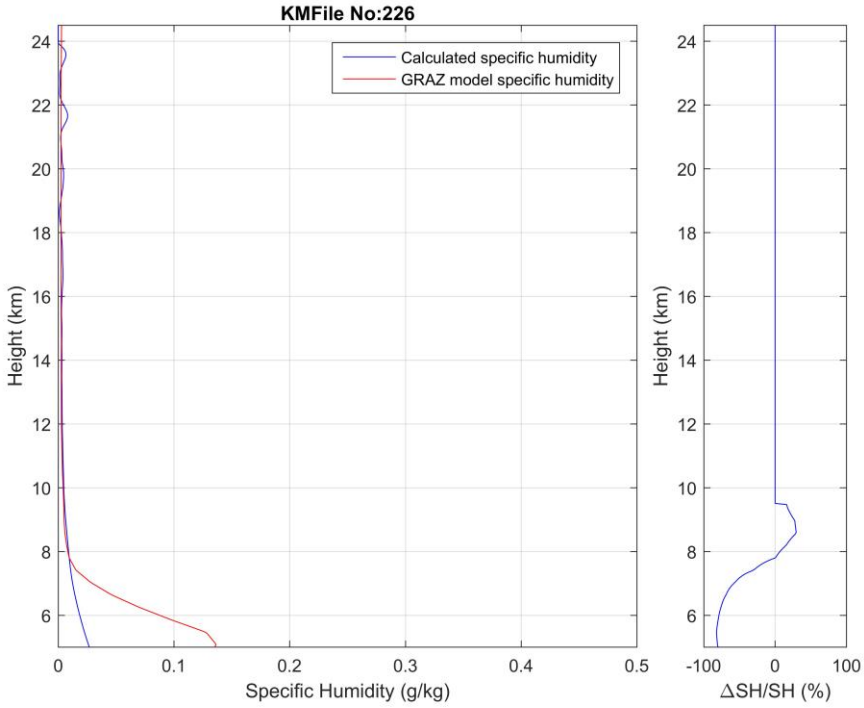

476

477 (D)

Figure 6. (A) The amplitude and phases for the 5 different KM frequencies. The mean latitude and longitude for the tangent point is -55.42 degrees -30.86 degrees for this setting occultation. (B) The pressure versus height. The blue curve is the retrieval while the red curve is the GRAZ model. (C) The temperature versus height. The blue curve is the retrieval while the red curve is the GRAZ model. (D) The specific humidity versus height. The blue curve is the retrieval while the red curve is the GRAZ model. Panels (B) to (D) all have a blue curve on the right side which is the relative difference between the retrieved values and the GRAZ model values.

The specific humidity is again determined as expected with the lowest precision, but it is still relative precise as long as all of the frequencies are present. The height at which the radio wave is absorbed in the atmosphere increase with increasing probing frequency leading to lower precision in the retrieved parameters.

491 **4.3 Simulation class statistics**

492 Simulations have been performed for 4 different classes corresponding to different
493 frequency systems and noise levels. Figure 7 shows the statistics for the retrieved
494 temperature for simulation class 2, 3 and 4. It seen that the noise increases the error levels
495 compared to the corresponding clear air case. The increase in the error levels are however
496 modest due to appropriate low pass filtering of the radio occulation amplitudes and
497 phases.

498

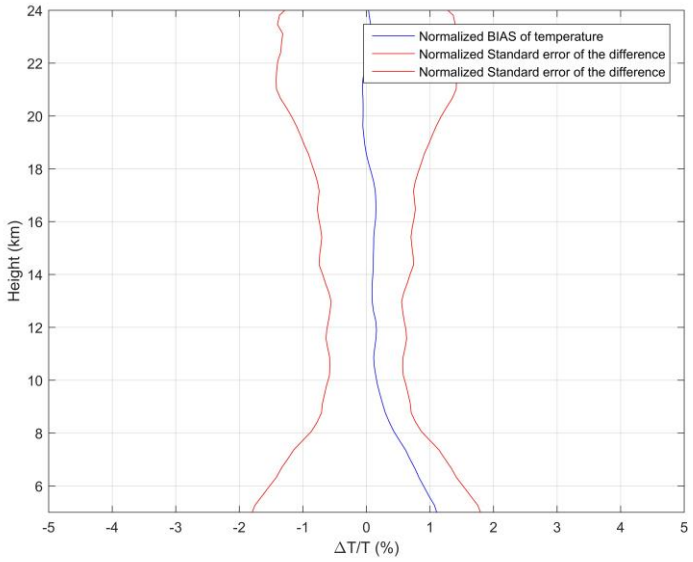

499 (A)

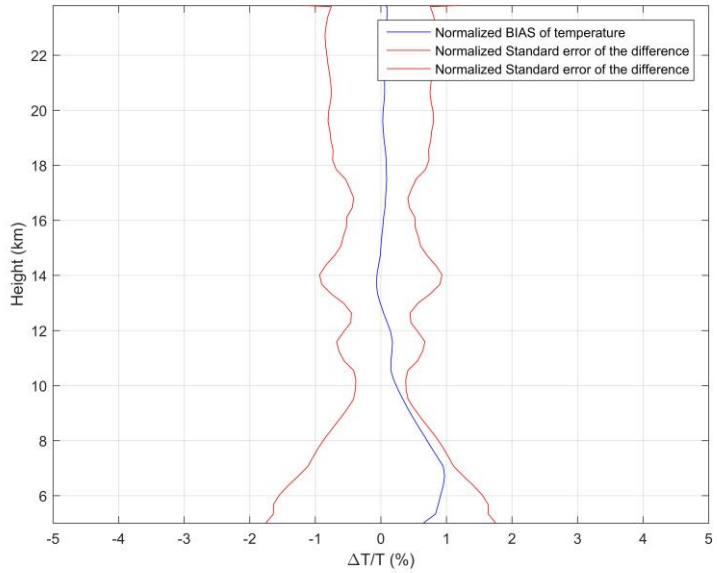

(B)

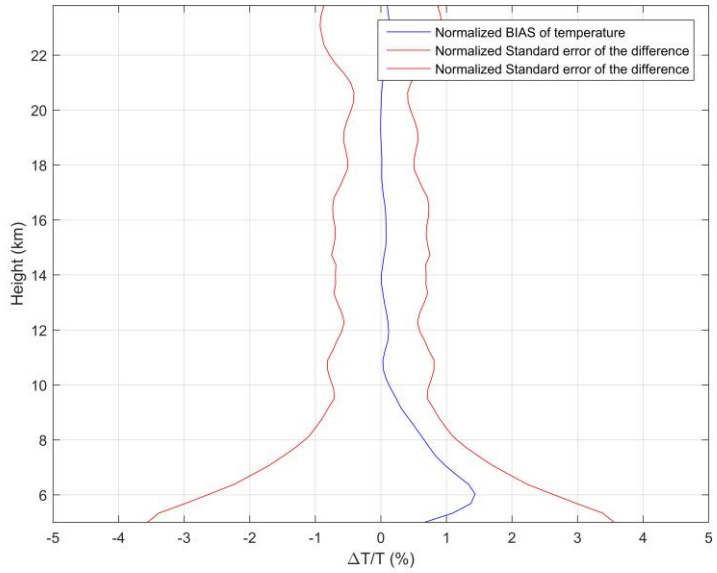

(C)

Figure 7. Panels (A) to (C). The normalized temperature bias (blue curve) and normalized standard error of the difference for temperature (red curve) in (%) as a function of height. (A) This is for Simulation Class 2. (B) This is for Simulation Class 3. (C) This is for Simulation Class 4.

In the current version of the retrieval chain extrapolated values are used when there are no imaginary refractivity values. The imaginary refractivity corresponding to the high frequencies in the KM range stops at a higher altitude than the values in the XK range. This is the reason for the higher error level seen for probing frequencies in the KM range. This issue can be solved using an extension of the imaginary refractivity (for these high frequency probing radio waves) to lower altitudes. This extension can be based on models in the same way bending angles are extended (due to a high noise level) at high altitudes using statistical optimization in GPS-LEO radio occultations. Work on this approach has been initiated.

It is seen that the bias and standard error of the difference all fall within an acceptable error level. The presented simulations and retrievals of LEO-LEO cross links radio occultations using high frequency probing radio waves have shown that this technique can be used even in challenging conditions to retrieval valuable information on important atmospheric parameters such as the atmospheric content of water vapor. Information that can not directly be extracted from standard GPS-LEO radio occulations. The presented retrieval chain is not a final operational chain and a number of things can be improved so errors presented here is higher than what can be accomplished. The technique discussed can also be used to retrieve other parameters such as the content of ozone. This is accomplished by adding additional probing frequencies.

5. Conclusion

We have in this study presented a wave optics based LEO-LEO retrieval chain. The new LEO-LEO radio occultation processing chain has been used on radio occultation simulations provided by the University of Graz. These radio occultations use 5 different XK or KM probing frequencies. Both radio occultations in clear air and in a turbulent cloudy atmosphere for frequencies in the XK and KM frequency range have been studied. The retrieval results were compared to the atmospheric parameters that are used to generate the inputs to the wave optics propagator. The error levels are as expected higher in the turbulent cloudy atmosphere compared to the error level in the clear air atmosphere. Based on these comparisons it can be concluded that the wave optics based retrieval chain gives good results for both XK and KM frequencies and the feasibility of the measurement concept has been shown. The results are in general a little better in the XK frequency range compared to the KM frequency. The reason for this is that the probing KM frequency waves stop at higher heights than the XK frequency waves. This cause a decrease in the precision of the solver results at low heights in the KM frequency based system of equations. The plots presenting the bias and standard deviation of the difference errors show an increase in the error level when the heights are decreasing. The reason for this is that there is no measurements at low altitudes and the complex refractivity values are therefore found from an extrapolation of the curves. This will in many cases lead to an error in the retrieved parameters at low altitudes and hence an increase in the error level. A method to overcome this has been mentioned in the paper. The results of the simulations in this study show that it is possible to retrieve atmospheric

parameters such as water vapor with out external information using a microwave LEO-LEO radio occultations technique. Future satellite missions could use this technique to measure these parameters which in general are considered to be a challenge to measure.

Acknowledgments

This work was supported by ESTEC Contract No. 16743/02/NL/FF. The authors wish to thank University of Graz for providing the simulated LEO-LEO radio occultations in the XK and KM frequency range. Data used in this paper can be obtained from the authors.

6. References

Benzon, H.-H., and P. Hoeg (2015), Wave propagation simulation of radio occultations based on ECMWF refractivity profiles, Radio Sci., 50, doi: 10.1002/2015RS005649.

Born, M., and E. Wolf, Principles of Optics, Cambridge Univ. Press, New York, 1999.

Eriksson, P., Jimenez, C., Murtagh, D., Elgered, G., Kuhn, T., Buhler, Measurement of tropospheric/stratospheric transmission at 10-35 GHz for H2O retrieval in low Earth orbiting satellite links. Radio Sci. Vol. 38, No. 4, 8069 doi:10.1029/2002RS002638 13 June 2003.

Fjeldbo, G., A. J. Kliore, and R. Eshlermann, The neutral atmosphere of Venus studied with the Mariner V radio occultation experiments, Astron. J., 76(2), 123-140, 1971.

Fritzer, J., G. Kirchengast, M. Pock, and V. Proschek (2010), End‐to‐End Generic Occultation Performance Simulation and Processing System version 5.5 (EGOPS 5.5) Software User Manual, Tech. Rep. ESA/ESTEC 1/2010, 490 pp., Wegener Cent. and IGAM/Inst. of Phys., Univ. of Graz, Graz, Austria.

Gorbunov, M.E., Canonical transform method for processing GPS radio occultation data in lower troposphere, Radio Science, 37(5), 10. 1029/2000RS002592, 9-1–9-10, 2002.

583 Gorbunov, M.E. and K. B. Lauritsen, Analysis of wave fields by Fourier Integral
584 Operators and its application for radio occultations, Radio Science, 2004, 39(4), RS4010,
585 doi:10. 1029/2003RS002971, 2004.
586
587 Gorbunov, M. E., and G. Kirchengast, Fluctuations of radio occultation signals in X/K
588 band in the presence of anisotropic turbulence and differential transmission retrieval
589 performance, Radio Sci., 42, RS4025, doi:10.1029/2006RS003544, 2007.
590
591 Gorbunov, M. E., G. Kirchengast, Processing X//K band radio occultation data in the
592 presence of turbulence, RADIO SCIENCE, VOL. 40, RS6001,
593 doi:10.1029/2005RS003263, 2005.
594
595 Gorbunov, M. E., G. Kirchengast, Fluctuations of radio occultation signals in X/K band
596 in the presence of anisotropic turbulence and differential transmission retrieval
597 performance, RADIO SCIENCE, VOL. 42, RS4025, doi:10.1029/2006RS003544, 2007.
598
599 Høeg, P., and G. Kirchengast, ACE+ Atmosphere and Climate Explorer based on GPS,
600 GALILEO, and LEO-LEO Radio Occultation, Proposal to ESA in Response to the
601 Second Call for Proposals for Earth Explorer Opportunity Missions, 2002.
602
603 Jensen, A. S., M. S. Lohmann, H-H Benzon and A. S. Nielsen, "Full Spectrum Inversion
604 of radio occultation signals," Radio Sci., 38(3), 1040, doi:10.1029/2002RS002763, 2003.
605

606 Jensen, A. S., M. S. Lohmann, A. S. Nielsen, and H.-H. Benzon, Geometrical optics
607 phase matching of radio occultation signals, Radio Sci., 39, RS3009, doi:
608 10.1029/2003RS002899, 2004.
609
610 Kirchengast, G., S. Schweitzer, J. Ramsauer, and J. Fritzer (2007), End-to-End Generic
611 Occultation Performance Simulator version 5.2 (EGOPSv5.2) Software User Manual
612 (Overview, Reference, and FileFormat Manual), Tech. Rep. ESA/ESTEC 4/2007,
613 Wegener Cent. And IGAM/Inst. of Phys., Univ. of Graz, Graz, Austria.
614
615 Kursinski, E. R, Leroy, S.S., and Herman, B, The Radio Occultation Technique, Terr.
616 Atmos. Oceanic Sci. 11, 53-114, 2000.
617
618 Kursinski, E. R., et al., A Microwave Occultation Observing System Optimized to
619 Characterize Atmospheric Water, Temperature, and Geopotential via Absorption, Journal
620 of Atmospheric and Oceanic Technology, 19, pp 1897-1914, 2002.
621
622 Liebe, H. J., MPM - an Atmospheric Millimeter-wave Propagation Model, International
623 Journal of Infrared and Millimeter Waves, vol. 10, No. 6, 1989.
624
625 Lohmann, M. S., A. S. Jensen, H-H Benzon, , and A. S. Nielsen, Application of window
626 functions for full spectrum inversion of cross-link radio occultation data, Radio Science
627 2006, doi 10.1029/2005RS003273.
628

629 Nielsen, A. S., M. S. Lohmann, P. Høeg, H.-H. Benzon, A. S. Jensen, T. Kuhn., C.
630 Melsheimer, S. A. Buehler, P. Eriksson, L. Gradinarsky, C. Jimenez, G. Elgered,
631 Characterization of ACE+ LEO-LEO Radio Occultation Measurements, ESTEC Contract
632 NO. 16743/02/NL/FF. 2003. This report can be obtained from the authors.
633
634 Hoeg, P., G. Kirchengast, ACE+: Atmosphere and Climate Explorer, Proposal to ESA,
635 see http://www.dmi.dk/fileadmin/Rapporter/SR/sr02-07.pdf, 2002.
636
637 Schweitzer, S., G. Kirchengast, M. Schwaerz, J. Fritzer, and M. E. Gorbunov,
638 Thermodynamic state retrieval from microwave occultation data and performance
639 analysis based on end-to-end simulations, J. Geophys. Res., 116, D10301,
640 doi:10.1029/2010JD014850, 2011.
641
642 Sorensen, D. C., Newton's Method with a Model Trust Region Modification, SIAM J.
643 Numer. Anal., 19(2), 409–426, 1982.
644